DOI 10.24425/aee.2025.154987

AC dielectric properties of antimony-germanate-borate optical glass rods co-doped with silver nanoparticles

OLEKSANDR BOIKO^{®1™}, JACEK MARIUSZ ŻMOJDA^{®2}, MARCIN KOCHANOWICZ^{®2}, TOMASZ RAGIŃ^{®2} JAKUB MARKIEWICZ^{®2}, KRZYSZTOF MARKOWSKI^{®2}, GRZEGORZ KAROL KOMARZYNIEC^{®1}

¹Lublin University of Technology Department of Electrical Engineering and Superconductivity Technologies 38A Nadbystrzycka St., 20-618 Lublin, Poland

²Białystok University of Technology, Faculty of Electrical Engineering 45D Wiejska St., 15-351 Białystok, Poland

e-mail: {⊠ o.boiko/g.komarzyniec}@pollub.pl, {j.zmojda/m.kochanowicz/tomasz.ragin/jakub.markiewicz}@pb.edu.pl, krzysztof.markowski@sd.pb.edu.pl

(Received: 04.02.2025, revised: 14.08.2025)

Abstract: The article presents the investigation of the AC dielectric properties of optical glass rods co-doped with Ag nanoparticles. The samples presented a molar composition of $20\text{Sb}_2\text{O}_3 - 30\text{GeO}_2 - (45 - x)\text{H}_3\text{BO}_3 - 5\text{Al}_2\text{O}_3 - x\text{Ag}$ and differed with Ag concentration x in the range of 0.1 mol·%–0.6 mol·% as well as geometric dimensions. The rods have been prepared by the standard melt-quenching technique. An impedance spectroscopy in the measurement frequency range of 4 Hz-8 MHz at room temperature was used to determine the dielectric properties of rods. The paper shows frequency characteristics for impedance, phase shift angle, resistance, conductivity, dissipation factor, and both components of permittivity. The samples demonstrate high resistance $(4.4 \times 10^6 < R < 2.0 \times 10^{11} \Omega)$ and mostly negative phase shift angle $(0 < \theta \le -90^{\circ})$, which indicates the purely dielectric nature of the materials and their capacitive character. Introducing Ag NPs into the rod's structure causes growth in the impedance of about 40-120%, amplifies the real part of the permittivity over fivefold, and increases the electrical conductivity from two to 4.5 times, depending on frequency f. Resistance, conductivity, dissipation factor, and imaginary part of permittivity demonstrate two-step saddle-shape dependencies that reflect dielectric and conduction processes between non- or partly oxidized or fully oxidized Ag nanoparticles separated by a glass matrix. The saddle points are different for low and high frequency regions, the values of which are next to 500 Hz and 5×10^5 Hz, respectively, referring to two relaxation times in the interphase polarization process. Hopping conductivity has been proposed as the charge transfer mechanism in nanocomposite rods.

Key words: co-doping, dielectric properties, hopping conductivity, nanocomposites, optical glasses



© 2025. The Author(s). This is an open-access article distributed under the terms of the Creative Commons Attribution-NonCommercial-NoDerivatives License (CC BY-NC-ND 4.0, https://creativecommons.org/licenses/by-nc-nd/4.0/), which permits use, distribution, and reproduction in any medium, provided that the Article is properly cited, the use is non-commercial, and no modifications or adaptations are made.

1. Introduction

Currently, intensive research is being conducted on a functional group of electrically conductive nanofiller-contained nano- and micro-composite materials of a typically dielectric nature for applications in electrical engineering, electronics, lighting, and sensor technologies, as well as aircraft technologies [1–5]. The structure of such materials is usually designed as a dielectric matrix containing in its volume appropriately distributed (most often randomly, depending on the production method) nanoparticles (NPs) of metals [6, 7], their alloys and oxides [8, 9], carbon nanotubes [10, 11], quantum dots [4] and other conducting compounds [12]. These types of composites can exist not only in a solid state but also in a liquid state. Then they are called nanofluids, while their phase structure (metal-dielectric) remains unchanged [13–15].

In most cases, the reason for such great interest in this group of materials with a conductive nanofiller-dielectric matrix (CNDM) phase structure is the decisive influence of the parameters and type of nanofiller on the physicochemical properties, especially the electrical, magnetic, and optical properties of the target composite. For example, in the case of co-polystyrene nanocomposites (NCs), the growth in the concentration of Co nanoparticles (65.5 nm in size) from 2 wt.% to 10 wt.% leads to a significant increase in the NC's saturation magnetization (from 2.82 emu/g to 8.22 emu/g respectively), magnetic remanence (from 0.1834 emu/g to 1.72 emu/g respectively) and coercivity of about 6.5%, which indicates the possibility of using the NC in electrical energy storage, photonic, and spintronic devices [16]. NCs with $(\text{FeCoZr})_x(\text{PbZrTiO}_3)_{100-x}$ phase structure demonstrate an electric percolation with a threshold of $x_c = 53 \pm 2$ at.%; the NCs below x_c show the direct dependence of conductivity vs. temperature (dielectric conduction), while above x_c – inverse dependence (metallic conduction) [17]. In the case of Au-CaCu₃Ti₄O₁₂ NCs, introducing the NPs of Au to a dielectric matrix introduces nonlinearity in the optical response of the tested nanomaterial [18]. Along with the Au concentration growth (6.9 at.% to 31.9 at.%), the nonlinear refractive index n_2 increases almost fourfold, while the absorption coefficient β – about 15 times.

Over the past three decades, the field of dielectric properties and processes in glasses and optical fibers doped with metallic nanoparticles or their alloys has experienced substantial growth. Based on bibliometric analyses from databases such as Scopus and Web of Science, it is estimated that approximately 1 500 to 2 000 scientific articles have been published on this topic since the mid-1990s, which is not a satisfactory result considering the enormous chemical and phase diversity of optical structures formed at that time.

Many studied dielectric issues such as interfacial effects and charge transport mechanisms [19], long-term stability and aging [20], scalability of fabrication techniques [21], nonlinear dielectric behavior [22], integration into functional devices [23], have not received full practical explanation and the creation of a unified theory. Moreover, understanding the mechanisms and dielectric processes of the materials presented in this work is very important from the point of view of their potential applications, especially in the energy-related sector in i.e. high-permittivity capacitors [24], displays and photovoltaic cells [25], energy storage devices [26], etc. Therefore, the research presented in the article focuses on describing the electrical properties of $20\text{Sb}_2\text{O}_3$ – 30GeO_2 – $(45-x)\text{H}_3\text{BO}_3$ – $5\text{Al}_2\text{O}_3$ –xAg (abbreviated as SGBAA), in particular the type and nature of electrical conductivity, dielectric losses, electrical permittivity, and the mechanism of dielectric polarization and relaxation as well as the effect of Ag NPs content on them. The research is also a preliminary step towards determining the correlation between the optical and dielectric properties of functional optical glasses doped with noble metal nanoparticles.

The research presented in the article concerns the determination of dielectric properties of SGBAA optical glass rods with a CNDM phase structure. Silver nanoparticles of size <100 nm were used as a conductive phase. These types of glasses have already been examined for their optical properties in our previous works [27–29]. Their amorphous nature was studied and confirmed by XRD measurements. The main findings have been regarding: the thermochemical reduction of Ag^+ ions during the melting process, a decrease in intensity in the near-infrared region with Ag concentration increasing, Ag NPs enhances luminescence properties, the main energy transfer between silver NPs and Er^{3+} ions (a rare-earth element necessary for producing optical fibers that operate effectively within a specific spectral range, e.g. in the emission range of $1.8-3.1~\mu m$, which is desirable in the construction of microlasers), etc. [29].

Within the framework of our long-term research strategy, the present study is intended to advance the understanding of the interdependence between dielectric and optical properties in optical glasses doped with metallic nanoparticles. The next phase of research in this series will focus on examining the effects of electrical permittivity on optical transmittance and refractive index, the impact of dielectric variations in the vicinity of glass—metal interfaces on localized plasmon resonances, as well as the influence of dielectric relaxation and stepwise electrical conduction on light scattering and attenuation phenomena across a range of frequencies.

2. Experimental

Set of four-type glass rods presenting molar composition of $20\text{Sb}_2\text{O}_3$ – 30GeO_2 – $(45-x)\text{H}_3\text{BO}_3$ – $5Al_2O_3$ -xAg, where $x = 0.0 \text{ mol}\cdot\%$, $0.1 \text{ mol}\cdot\%$, $0.3 \text{ mol}\cdot\%$, and $0.6 \text{ mol}\cdot\%$ have been produced using the standard melt-quenching technique [30, 31]. The high purity reagent-grade powders employed in this study were procured from commercial suppliers as follows: antimony trioxide (Sb2O3, 99.99%), germanium dioxide (GeO2, 99.98%) and silver (Ag, 99.5%) from Sigma-Aldrich KGaA, Germany; boric acid (H3BO3, < 99.98%) from Chempur Ltd., Poland; and aluminum oxide (Al2O3, < 98.50%) from Avantor Performance Materials, Poland. The powders were mixed and placed in a quartz crucible, then melted in an electric furnace at 1 300°C for 1.5 h in the atmosphere of air. The next step was melt pouring into a brass cylinder-shaped form (11 mm in diameter of hole, 52 mm in height) at room temperature (RT) and immediately placing it in the stress reliever machine for 1 h at 350°C. Then the machine was switched off, and the preform was cooling down until it reached RT. The preforms were further polished to obtain a smooth surface and uniform diameter along their entire length. The glass rods were extracted from the preforms using an SG Controls extraction tower at 650°C. The following rod diameter ranges were obtained: set #1: 1.47–1.58 mm for SGBAA with no Ag NPs; set #2: 1.12–1.27 mm for $x = 0.1 \text{ mol} \cdot \%$; set #3: 1.10–1.16 mm for $x = 0.3 \text{ mol}\cdot\%$; and set #4: 0.84–1.00 mm for $x = 0.6 \text{ mol}\cdot\%$.

To perform dielectric measurements, the rods were cut into smaller pieces with lengths ranging from 7.94 mm to 15.50 mm. The analysis of literature sources [32,33] and our previous experience in studying the dielectric properties of nanomaterials with the CNDM phase structure [8,34] indicated the possibility of observing interfacial and dipole polarization in the megahertz range of measurement frequencies or lower. Therefore, the dielectric spectroscopy method was used for the dielectric characterization of SGBAA composite rods using the IM3536 LCR meter (Hioki Inc., Japan) meter measuring AC electrical parameters of materials in the range of 4 Hz–8 MHz.

The parameters studied in the RT were: complex impedance Z, phase shift angle θ , resistance R estimated with the use of parallel equivalent circuit arrangement, dissipation factor $\tan \delta$, and conductivity σ . A thick layer of silver paste was also applied to the side surfaces of individual samples to improve the electrical contact.

Electrical parameters such as complex impedance Z, phase shift angle θ , resistance R estimated with the use of parallel equivalent circuit arrangement, dissipation factor $\tan \delta$, and conductivity σ , were measured with use of IM3536 LCR meter (Hioki Inc., Japan) for the frequencies ranging from 4 Hz to 8 MHz at the RT.

3. Results and discussion

3.1. Overall electric performance of SGBAA rods

Figure 1(a) shows the frequency characteristics of impedance Z for selected SGBAA samples. Region A (the enlargement of which is shown in Fig. 1(b)) shows the variability of the impedance change trend after reaching characteristic frequencies in the 10–30 Hz range. In the case of frequencies f higher than 30 Hz, the impedance rapidly decreases along with f. Figure 1(c) demonstrates an exemplary frequency region B of impedance descending $(1.0 \times 10^5 \text{ Hz} < f < 4.5 \times 10^5 \text{ Hz})$. It also shows clearly that introducing Ag NPs into the glass matrix increases Z by at least 40%. The lowest x value gives the largest impedance increase, which may seem unusual for bulk CNDM-type structures and will be further discussed in Section 3.2.

Figure 1(d) presents the frequency dependence of phase shift angle θ . There are two observable frequency regions in which θ behaves clearly differently – low frequencies up to about 100 Hz (which would coincide with frequency region A in Fig. 1(a)) and a region of higher frequencies above 100 Hz.

Our previous experience with the impedance spectroscopy of NCs such as $(\text{FeCoZr})_x(\text{PbZrTiO}_3)_{100-x}$ [35], $(\text{CaF}_2)_x(\text{PbZrTiO}_3)_{100-x}$ [36], and $\text{Cu}_x(\text{SiO}_2)_{100-x}$ [37], associates the occurrence of a positive phase shift with the hopping mechanism of AC conductivity in the material. Hopping conductivity considers electron tunneling between adjacent NPs due to the application of an external electric field. After changing the field direction to the opposite one, the electron remains in the nanoparticle for a short time of the order of 10^{-13} s (also dependent on the frequency) and only then makes another hop (returns to the previous nanoparticle or the next one, details of the hopping theory in CNDM structures are presented in [17]). Such a delay causes the appearance of positive θ values. SGBAA glass rods also possess CNDM phase structure, whereas the potential wells can be considered Ag NPs, meaning the hopping conductivity model can be applied to them.

Figure 1(d) demonstrates a set of measurement points with θ values $\approx 0^{\circ}$ around f=10 Hz. It also corresponds to the frequency-limited, purely resistive state of the NC. Generally, the equivalent circuit of most real-functional materials can be represented as a series connection of electronic elements such as a resistor, capacitor, and an inductor. In this circuit, 0° of phase shift indicates the voltage resonance phenomenon, described in the example of metal-dielectric NCs in [38].

In the case of frequencies > 10 Hz, the θ is negative, which indicates the capacitive character of the samples. After exceeding 100 Hz, the material's behavior changes into pure capacitive ($\theta \approx -90^{\circ}$).

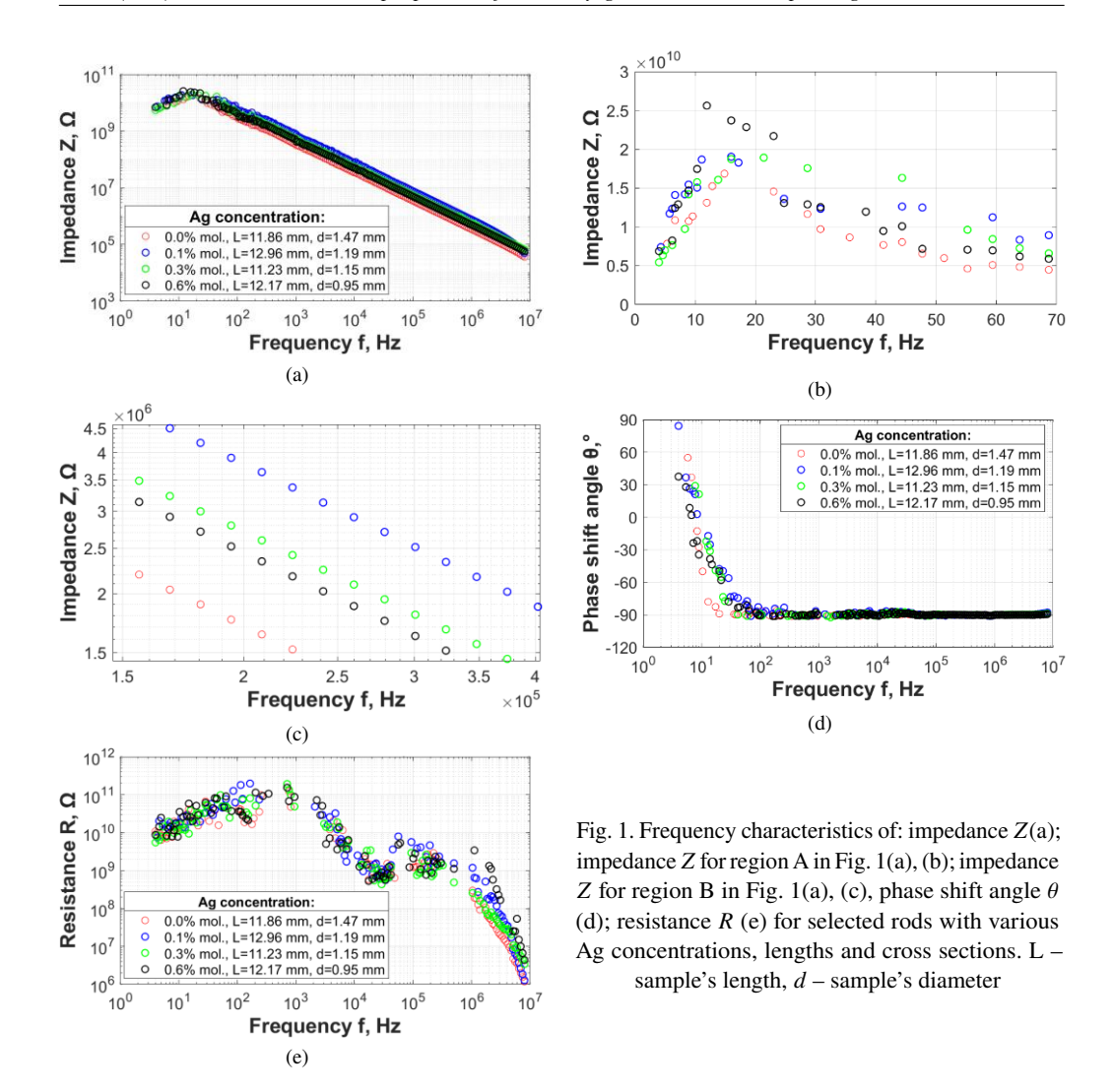


Figure 1(e) shows the frequency dependency of the samples' resistance. From this figure, it can clearly be seen that characteristics displays the form of two humps with the highest values registered around the frequencies of $f_1 = 5 \times 10^2$ Hz and $f_2 = 5 \times 10^5$ Hz. Between these frequencies, there is a transition region of resistance in which a local minimum value is reached around $f = 3 \times 10^4$ Hz. More explanation on this situation is presented in Section 3.2. All samples demonstrate a purely dielectric nature.

3.2. AC conductivity analysis

Figures 2(a–d) present frequency characteristics of conductivity σ of SGBAA rods as well as fitting lines for those datasets. It can clearly be seen that σ demonstrates a two-step increasing tendency: a) the low-frequency region (LFR) from 4 Hz to the limit frequency $f_{\rm lim}$, and from

 $f_{\rm lim}$ to 8 MHz, that is called the high-frequency region (HFR). For all four cases, $f_{\rm lim}$ is different. The best possible fitting results (with the highest coefficients of determination for LFR ($R_{\rm LFR}^2$) and HFR ($R_{\rm LFR}^2$) presented in Table 1) for both region datasets have been obtained with use of exponential function $\sigma = \sigma_0 \cdot \exp(n \cdot f)$ approximation, where σ_0 – approximation coefficient depending on the type of interface on which conduction occurs, and n – exponential approximation power index. In Figs. 2(a–d), the solid fitting lines refer to the LFR, and dashed ones – HFR. In the case of Fig. 2(b), the approximation curves are characterized by the smallest $R_{\rm LFR}^2$ and $R_{\rm HFR}^2$ coefficients and are the least well-fitted to the experimental results. However, they can be considered appropriate because they fully follow their trend and correspond to the proposed theory.

The calculated approximation parameters are presented, and experimentally estimated f_{lim} for SGBAA samples are presented in Table 1. Coefficients σ_{01} and n_1 corresponds to the LFR, and σ_{02} and n_2 – HFR, respectively. The high level of agreement between the approximation and experimental results testifies that the total conductivity σ can be expressed as:

$$\sigma = \sigma_{01} \cdot e^{n_1 \cdot f_1} + \sigma_{02} \cdot e^{n_2 \cdot f_2},\tag{1}$$

where frequencies f_1 and f_2 belong to the LFR and HFR, respectively.

Both LFR and HFR regions can be divided into two characteristic subregions (that is better observable in the fitting curves): flat subregion of insignificant (almost stability-like) frequency dependence of σ (subregions S1 and S3 in Fig. 2(a)) and subregion of strong dependence σ on f (subregions S2 and S4 in Fig. 2(a)). In accordance with the electrochemical impedance spectroscopy approach, S1 and S3 correspond to the high-resistance grain boundary conductivity, and S2 and S4 – short-range hopping mobilities between Ag grains [39, 40]. However, due to the high difference between S1 and S3 levels (about 1.5 orders of magnitude), it can be assumed that S1 regards the grain boundaries of oxidized Ag NPs (OAN, see Fig. 1(e), where the sample's resistance in LFR is also much higher than resistance in HFR), and S3 – grain boundaries of non-oxidized Ag NPs (NOAN). Then S2 and S4 are subregions, where the carrier mobilities take place between adjacent OAN and NOAN grains, respectively.

Ag conc. mol.%	σ_{01}	n_1	σ_{02}	n ₂	$R_{ m LFR}^2$	R _{HFR}	$f_{ m lim}, \ m Hz$
0.0	2E-10	2E-04	7E-09	1E-06	0.7707	0.8957	2.92E+04
0.1	9E-10	2E-04	6E-08	1E-06	0.5681	0.4169	4.20E+04
0.3	4E-10	2E-04	1E-08	8E-07	0.8301	0.9917	3.63E+04
0.6	5E-10	2E-04	1E-08	9E-07	0.8521	0.9754	2.92E+04

Table 1. Fitting parameters for conductivity characteristics

Figures 2(e) and 2(f) describe the influence of Ag content on the electrical conductivity of SGBAA samples. Figure 2(e) shows a significant increase in σ after introducing Ag NPs into the SGBA glass matrix. For both LFR and HFR subregions, the highest σ value demonstrates samples with 0.1 mol.%. Then, σ decreases while concentration goes up. Such a situation (when

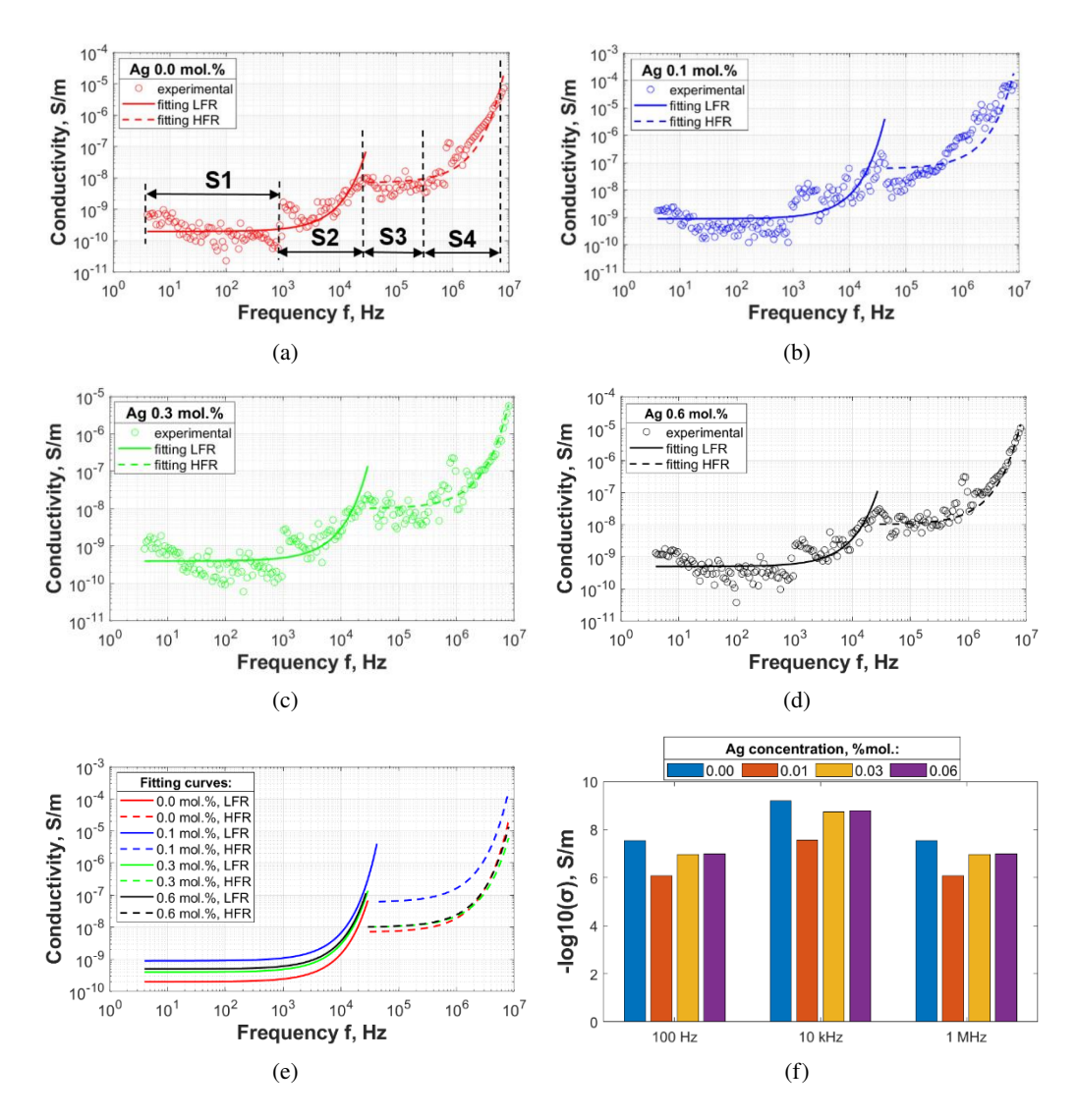


Fig. 2. Conductivity investigation for SGBA glass rods including Ag nanoparticles with concentrations: (a) 0.0% mol.; (b) 0.1% mol.; (c) 0.3% mol.; (d) 0.6% mol., as well as (e) fitting curves, and (f) bar chart for conductivity vs. Ag concentration for different frequencies

with only small concentrations of conductive NPs the greatest increase in the conductivity of the nanocomposite occurs) is most often reported in the case of CNDM-structured nanofluids [41–43], and less frequently in the case of bulk CNDM NCs [44, 45]. Figure 2(f) includes σ measurements for selected frequencies f (100 Hz, 10 kHz, 1 MHz) for all sample concentrations. The trend of σ behavior is fully consistent with that shown in Fig. 2(e). Moreover, it fully reflects the tendency of f_{lim} vs. Ag concentration from Table 1.

3.3. Dissipation factor and permittivity investigation

Figures 3(a-c) describe the dielectric processes in the SGBAA glass rods. The frequency dependences of the dissipation factor $\tan \delta$ (Fig. 3(a)), real ε' (Fig. 3(b)) and imaginary ε'' (Fig. 3(c)) parts of complex permittivity ε :

$$\varepsilon = \varepsilon' = i \cdot \varepsilon. \tag{2}$$

Loss factor $\tan \delta$ reflects energy losses regarding dielectric's conduction mechanisms and dipole relaxation phenomena in the NCs, and combines both components of permittivity:

$$\tan \delta = \varepsilon/\varepsilon'. \tag{3}$$

 $\tan \delta(f)$ dependencies majorly resemble the shape of the curves from $\varepsilon''(f)$ characteristics. The imaginary part of permittivity can be calculated as:

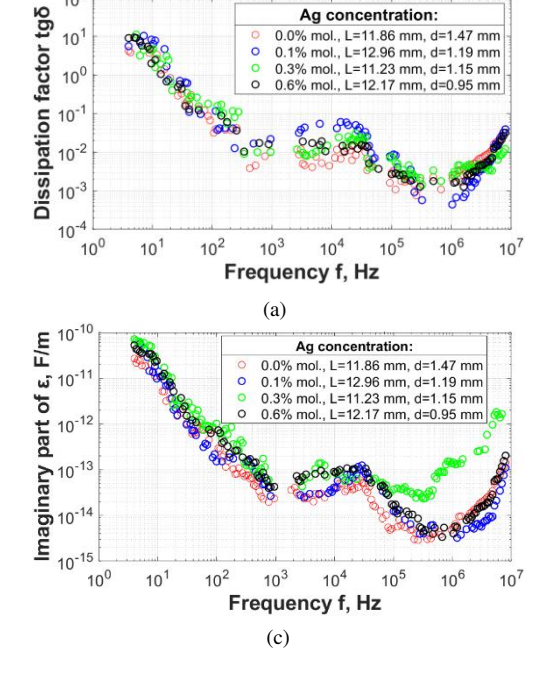
$$\varepsilon'' = \sigma/\omega = \sigma/2\pi f,\tag{4}$$

where ω is a pulsation.

10

10

Figure 3(a) shows a two-stage reduction of the value until reaching a frequency of about 10⁶ Hz, after which it starts to increase up to 1.5 orders of magnitude. The first reduction region 4 Hz–220 Hz is directly related to the strong frequency dependence of the phase shift angle θ (Fig. 1(d)), which varies almost in the full possible range of its values, i.e. from almost +90° $(x = 0.1 \text{ mol}\cdot\%)$ to nearly -90° (all samples). Such behavior, together with a clearly visible maximum of ε' in the lowest measurement frequencies (Fig. 3(b)), points also to the interface



Ag concentration:

0.0% mol., L=11.86 mm, d=1.47 mm 0.1% mol., L=12.96 mm, d=1.19 mm

0.3% mol., L=11.23 mm, d=1.15 mm

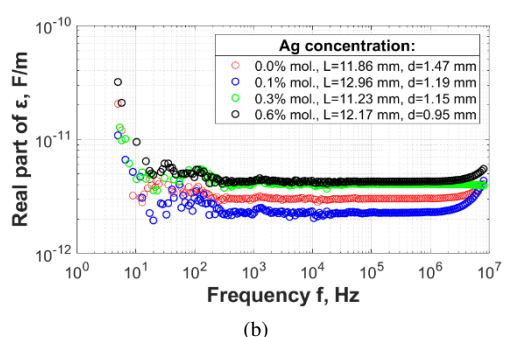


Fig. 3. Frequency dependencies of: (a) dissipation factor $\tan \delta$; (b) real part of the permittivity ε' , and (c) imaginary part of the permittivity ε'' of SGBAA rods with different Ag NPs concentration

polarization (alternatively-called space charge), which takes place at the electric contact-dielectric medium interlayer. It can be assumed that two characteristic stability regions correspond to the energy losses at the grain boundaries between oxidized (f range from about 220 Hz-3.91 kHz) and non-oxidized (f range from about $1.81 \cdot 10^5$ Hz- $1.60 \cdot 10^6$ Hz) NPs. High-frequency growing regions (> 10^6 Hz) of $\tan \delta$ and ε' , in accordance with the modern relevant theory of dielectric polarization [46,47], indicate dipolar-type polarization in the SGBAA glass rods.

Figure 3(b) demonstrates mainly flat characteristics (regime of stability) with the significant $\varepsilon'(f)$ dependency only for frequencies < 220 Hz, and, in the case of SGBAA samples with $x = 0.1 \text{ mol} \cdot \%$ and $x = 0.6 \text{ mol} \cdot \%$, for the frequencies above $1.6 \cdot 10^6$ Hz. The values of ε' were calculated from (3). Figure 3(c) presents the frequency characteristic of the imaginary part of permittivity ε'' , which resembles the behavior of curves and characteristic frequency regions as shown in Fig. 3(a).

4. Conclusions

The nanocomposite materials, which are SGBAA glasses in the form of rods, were manufactured via a nonstandard, as for the functional nanostructures, melt-quenching technique, mostly associated with the production of optical fibers. The samples varied with Ag NPs' content from $0.1 \text{ mol}\cdot\%$ to $0.6 \text{ mol}\cdot\%$.

The NCs were examined for their AC dielectric properties and the effect of Ag content on them. As expected, all samples exhibit a strongly dielectric nature. The analysis of the frequency dependence of conductivity indicates a predominantly hopping charge transfer mechanism in the samples. In this situation, the charge carriers move stepwise between adjacent Ag nanoparticles, which can be additionally oxidized or without an oxide shell. The oxide shell constitutes an additional energy barrier to be overcome by the charge carriers, therefore, the conductivity of the samples in the first stage (low-frequency region) is noticeably lower than in the second one.

A similar two-step decreasing trend was also observed in the dissipation factor and permittivity of the samples. The behavior of the curves of real and imaginary parts of permittivity indicates two mechanisms of dielectric polarization – interfacial and dipole, but the interfacial polarization takes place not only in the interface between the electrical contact and the sample's cross-section surface, but also at the Ag grain boundaries.

Introducing Ag NPs into the structure of optical glass increases the impedance and the real part of the permittivity (except for the concentration of 0.1 mol·%) and noticeably reduces the electrical conductivity. As future supplementary studies, microscopic tests (SEM, TEM) can be defined regarding the determination of the distribution of silver nanoparticles in the glass matrix, and the examination of the oxidation degree of conductive grains. The latter may be difficult to implement considering the selected material production method, so it can be replaced with e.g. vacuum RF magnetron sputtering (for some techniques, of testing the chemical composition, such as XPS spectroscopy, ultra-thin layers of the tested materials are needed). SGBAA granular structures should also be investigated with respect to the influence of temperature and higher frequencies, e.g. radio frequencies or higher, on their properties and electrical phenomena (resonance, percolation, atomic polarization) and energetic processes occurring in them.

The SGBAA nanocomposites represent a promising class of nanostructured materials suitable for both experimental and theoretical studies focused on electrical conductivity mechanisms, polarization behavior, and dielectric relaxation phenomena. These properties make them viable not only for applications in sensor technology, biomedical systems, and optics, but also in energy-related fields, including high-permittivity capacitors, displays and photovoltaic devices, energy storage systems, and advanced insulation components for high-voltage power networks.

Acknowledgements

Oleksandr Boiko would like to express his heartfelt thanks to the employees of the Department of Photonics, Electronics and Lighting Technology at the Białystok University of Technology for the opportunity to complete a research internship in 2024 as part of the project "VIA CARPATIA Universities of Technology Network named after the President of the Republic of Poland Lech Kaczyński". The current publication is the scientific and research result of the internship and the fruitful cooperation of scientists from the Lublin University of Technology and the Białystok University of Technology.

References

- [1] Jalali A., Kheradmandkeysomi M., Buahom P., Gupta T., Habibpour S., Omranpour H., Yu A.P., Sain M., Park C.B., Engineering lightweight Poly(lactic acid) graphene nanoribbon nanocomposites for sustainable and stretchable electronics: Achieving exceptional electrical conductivity and electromagnetic interference shielding with enhanced thermal conductivity, Carbon, vol. 226, 119196 (2024), DOI: 10.1016/j.carbon.2024.119196.
- [2] Wang S.J., Xu P., Xu X.Y., Kang D., Chen J., Li Z., Huang X.Y., *Tailoring the Electrical Energy Storage Capability of Dielectric Polymer Nanocomposites via Engineering of the Host–Guest Interface by Phosphonic Acids*, Molecules, vol. 27, no. 21, 7225 (2022), DOI: 10.3390/molecules27217225.
- [3] Aquino F.T., Caixeta F.J., de Oliveira Lima K., Kochanowicz M., Dorosz D., Gonçalves R.R., *Broadband NIR emission from rare earth doped-SiO*₂-*Nb*₂*O*₅ *and SiO*₂-*Ta*₂*O*₅ *nanocomposites*, Journal of Luminescence, vol. 199, pp. 138–142 (2018), DOI: 10.1016/j.jlumin.2018.03.018.
- [4] Ja'farawy M.S.A., Thirumalai D., Lee J.W., Jung H.S., Chang S.C., Yoon J.H., Kim D.H., *Graphene quantum dot nanocomposites: electroanalytical and optical sensor technology perspective*, Journal of Analytical Science and Technology, vol. 14, no. 1, 29 (2023), DOI: 10.1186/s40543-023-00393-2.
- [5] Bijulin Greety D.J., Wessley G.J.J., A study on EMI shielding in aircraft: introduction, methods and significance of using electrospun nanocomposites, Journal of Space Safety Engineering, vol. 11, no. 1, pp. 150–160 (2024), DOI: 10.1016/j.jsse.2024.01.001.
- [6] Nur-E-Alam M., Basher M.K., Vasiliev M., Das N., Physical Vapor-Deposited Silver (Ag)-Based Metal-Dielectric Nanocomposites for Thin-Film and Coating Applications, Applied Sciences, vol. 11, no. 15, 6746 (2021), DOI: 10.3390/appl1156746.
- [7] Niguma R., Matsuyama T., Wada K., Okamoto K., Novel Plasmonic Metamaterials Based on Metal Nano-Hemispheres and Metal-Dielectric Composites, Photonics, vol. 11, no. 4, 356 (2024), DOI: 10.3390/photonics11040356.
- [8] Boiko O., Drozdenko D., Minárik P., Dielectric properties, polarization process, and charge transport in granular (FeCoZr)_x(Pb(ZrTi)O₃)_(100-x) nanocomposites near the percolation threshold, AIP Advances, vol. 12, no. 2 (2022), DOI: 10.1063/6.0001356.

- [9] Meng X.X., Zhou W.Y., Chen X.L., Kong F.R., Zhao J.H., Li W.W., Zhang Y.Q., Wang F., Yuan M.X., Synergistic regulation of intra-particle and inter-particle polarizations in BaTiO₃@Al₂O₃/PVDF nanocomposites towards boosted overall dielectric properties, Materials Today Chemistry, vol. 43, 102492 (2025), DOI: 10.1016/j.mtchem.2024.102492.
- [10] Kim M.N., Lee H., Cho J., Oh M.J., Kim S.H., Jang J.U., Kim S.Y., Facile engineering strategy to control polymer chain structure for enhanced dispersion, electrical and sensing properties of nanocomposites, Composites Part A: Applied Science and Manufacturing, vol. 176, 107827 (2024), DOI: 10.1016/j.compositesa.2023.107827.
- [11] Kolodziej L., Iwasińska-Kowalska O., Wróblewski G., Giżewski T., Jakubowska M., Lekawa-Raus A., *Hydrogels and Carbon Nanotubes: Composite Electrode Materials for Long-Term Electrocardiography Monitoring*, Journal of Functional Biomaterials, vol. 15, no. 5, 113 (2024), DOI: 10.3390/jfb15050113.
- [12] Tong Y., Liu Y.M., Zhang D., Wu J.W., Lai J.G., Ju S.S., Li J.A., Li Y.T., Liu J.C., Effect of interfacial area and particle size on the microstructure and dielectric properties of BaTiO₃-SiO₂ nanocomposites, Journal of Materials Science: Materials in Electronics, vol. 35, no. 12, 843 (2024), DOI: 10.1007/s10854-024-12614-4.
- [13] Biliak K., Nikitin D., Ali-Ogly S., Protsak M., Pleskunov P., Tosca M., Sergievskaya A., Cornil D., Cornil J., Konstantinidis S., Kosutová T., Cernochová Z., Stepánek P., Hanus J., Kousal J., Hanyková L., Krakovsky I., Choukourov A., *Plasmonic Ag/Cu/PEG nanofluids prepared when solids meet liquids in the gas phase*, Nanoscale Advances, vol. 5, no. 3, pp. 955–969 (2023), DOI: 10.1039/D2NA00785A.
- [14] Boiko O., Stryczewska H.D., Komarzyniec G.K., Ebihara K., Aoqui S., Yamazato M., Zagirnyak M., *Key factors enhancing the electrical properties of nanofluids. A mini-review of the applications in the energy-related sectors*, Archives of Electrical Engineering, vol. 73, no. 4, pp. 1137–1160 (2024), DOI: 10.24425/aee.2024.152115.
- [15] Nikitin D., Biliak K., Pleskunov P., Ali-Ogly S., Cervenkova V., Carstens N., Adejube B., Strunskus T., Cernochova Z., Stepanek P., Bajtosova L., Cieslar M., Protsak M., Tosca M., Lemke J., Faupel F., Biederman H., Vahl A., Choukourov A., Resistive Switching Effect in Ag-poly(ethylene Glycol) Nanofluids: Novel Avenue Toward Neuromorphic Materials, Advanced Functional Materials, vol. 34, no. 12, 2310473 (2024), DOI: 10.1002/adfm.202310473.
- [16] Nasralla N.H.S., Mousa S.M., El-Bassyouni G.T., El Komy G.M., *Synthesis of cobalt nanoparticles in polystyrene matrix enhanced optical, dielectric, and magnetic properties*, Surfaces and Interfaces, vol. 48, 104291 (2024), DOI: 10.1016/j.surfin.2024.104291.
- [17] Koltunowicz T.N., Zukowski P., Boiko O., Saad A., Fedotova J.A., Fedotov A.K., Larkin A.V., Kasiuk J., AC Hopping Conductance in Nanocomposite Films with Ferromagnetic Alloy Nanoparticles in a PbZrTiO₃ Matrix, Journal of Electronic Materials, vol. 44, no. 7, pp. 2260–2268 (2015), DOI: 10.1007/s11664-015-3685-9.
- [18] Ning T., Lu H., Zhou Y., Man B., Decrease and enhancement of third-order optical nonlinearity in metal-dielectric composite films, Applied Physics Letters, vol. 112, no. 15, 151904 (2018), DOI: 10.1063/1.5022129.
- [19] Jiménez J.A., Lysenko S., Vikhnin V.S., Liu H., Interfacial Effects in the Relaxation Dynamics of Silver Nanometal-Glass Composites Probed by Transient Grating Spectroscopy, Journal of Electronic Materials, vol. 39, no. 1, pp. 138–143 (2010), DOI: 10.1007/s11664-009-0961-6.
- [20] Louzguine-Luzgin D.V., Jiang J., On Long-Term Stability of Metallic Glasses, Metals, vol. 9, 1076 (2019), DOI: 10.3390/met9101076.
- [21] Dhar A., Choudhury N., Sen R., Advancements in fabrication technology for rare-earth doped optical fibers: A retrospective analysis, Optics Communications, vol. 577, 131463 (2025), DOI: 10.1016/j.optcom.2024.131463.

- [22] Brückner V., Nonlinearities in Glass Fibers, in Elements of Optical Networking, Springer Vieweg, Wiesbaden (2024).
- [23] Kadathala L., Park Y.O., Kim J.H., Lee J.S., Won J.C., Kim Y.H., Han W.T., Kim B.H., *Low dielectric properties of alkali-free aluminoborosilicate fiber glasses for PCB applications at 10 GHz*, Scientific Reports, vol. 14, no. 1, 27749 (2024), DOI: 10.1038/s41598-024-79456-2.
- [24] Wang L., Zhang Q.M., Du J., Structural characteristics and dielectric properties of glass-ceramic nanocomposites of (Pb,Sr)Nb₂O₆-NaNbO₃-SiO₂, Transactions of Nonferrous Metals Society of China, vol. 20, no. 8, 1434–1438 (2010), DOI: 10.1016/S1003-6326(09)60317-4.
- [25] Bahgat A.A., Moustafa M.G., Shaisha E.E., Enhancement of Electric Conductivity in Transparent Glass-Ceramic Nanocomposites of Bi₂O₃-BaTiO₃ Glasses, Journal of Materials Science & Technology, vol. 29, no. 12, pp. 1166–1176 (2013), DOI: 10.1016/j.jmst.2013.08.005.
- [26] Zhang J.S., Hou D.J., Wang J., Liu H.X., Huang C., Cheng S., Zhou L., Shen Z.H., Li B.W., Zhou J., Zhang P.C., Chen W., Bioinspired Dielectric Nanocomposites with High Charge-Discharge Efficiency Enabled by Superspreading-Induced Alignment of Nanosheets, ACS Applied Materials & Interfaces, vol. 16, no. 11, pp. 14162–14170 (2024), DOI: 10.1021/acsami.3c19546.
- [27] Czajkowski K., Optical properties of antimony-borate glass rods co-doped with Eu³⁺/Ag⁺ ions, Photonics Letters of Poland, vol. 13, no. 4, 94 (2021), DOI: 10.4302/plp.v13i4.1119.
- [28] Zmojda J., Kochanowicz M., Miluski P., Baranowska A., Pisarski W.A., Pisarska J., Jadach R., Sitarz M., Dorosz D., *Structural and optical properties of antimony-germanate-borate glass and glass fiber co-doped Eu*³⁺ *and Ag nanoparticles*, Spectrochim Acta A Mol Biomol Spectrosc, vol. 201, pp. 1–7 (2018), DOI: 10.1016/j.saa.2018.04.051.
- [29] Zmojda J., Kochanowicz M., Miluski P., Baranowska A., Basa A., Jadach R., Sitarz M., Dorosz D., *The influence of Ag content and annealing time on structural and optical properties of SGS antimony-germanate glass doped with Er*³⁺ *ions*, Journal of Molecular Structure, vol. 1160, pp. 428–433 (2018), DOI: 10.1016/j.molstruc.2018.02.030.
- [30] Veber A., Lu Z., Vermillac M., Pigeonneau F., Blanc W., Petit L., Nano-Structured Optical Fibers Made of Glass-Ceramics, and Phase Separated and Metallic Particle-Containing Glasses, Fibers, vol. 7, 105 (2019), DOI: 10.3390/fib7120105.
- [31] Zmojda J., Miluski P., Kochanowicz M., *Nanocomposite Antimony-Germanate-Borate Glass Fibers Doped with Eu*³⁺ *Ions with Self-Assembling Silver Nanoparticles for Photonic Applications*, Applied Sciences, vol. 8, 790 (2018), DOI: 10.3390/app8050790.
- [32] Sun H.B., Zhang H.L., Liu S.T., Ning N.Y., Zhang L.Q., Tian M., Wang Y., Interfacial polarization and dielectric properties of aligned carbon nanotubes/polymer composites: The role of molecular polarity, Composites Science and Technology, vol. 154, pp. 145–153 (2018), DOI: 10.1016/j.compscitech.2017.11.008.
- [33] Prasad V., Suresh B., Kostrzewa M., Gandhi Y., Ingram A., Reddy A.S.S., Kumar V.R., Veeraiah N., Dielectric dispersion, dipolar relaxation and a.c. conduction phenomena of NiO doped lead bismuth silicate glass system, Journal of Non-Crystalline Solids, vol. 500, pp. 460–467 (2018), DOI: 10.1016/j.jnoncrysol.2018.09.002.
- [34] Boiko O., Dielectric properties of metallic alloy FeCoZr-dielectric ceramic PZT nanostructures prepared by ion sputtering in vacuum conditions, Proceedings of 5th Global Conference on Polymer and Composite Materials (PCM 2018), Kitakyushu, Japan, vol. 369, 012016 (2018).
- [35] Zukowski P., Koltunowicz T.N., Boiko O., Bondariev V., Czarnacka K., Fedotova J.A., Fedotov A.K., Svito I.A., *Impedance model of metal-dielectric nanocomposites produced by ion-beam sputtering in vacuum conditions and its experimental verification for thin films of* $(FeCoZr)_X(PZT)_{(100-x)}$, Vacuum, vol. 120, pp. 37–43 (2015), DOI: 10.1016/j.vacuum.2015.04.035.

- [36] Zukowski P., Koltunowicz T.N., Bondariev V., Fedotov A.K., Fedotova J.A., *Determining the percolation threshold for* $(FeCoZr)_X(CaF_2)_{(100-x)}$ *nanocomposites produced by pure argon ion-beam sputtering*, Journal of Alloys and Compounds, vol. 683, pp. 62–66 (2016), DOI: 10.1016/j.jallcom.2016.05.070.
- [37] Koltunowicz T.N., Zukowski P., Czarnacka K., Bondariev V., Boiko O., Svito I.A., Fedotov A.K., *Dielectric properties of nanocomposite* $(Cu)_x(SiO_2)_{(100-x)}$ *produced by ion-beam sputtering*, Journal of Alloys and Compounds, vol. 652, pp. 444–449 (2015), DOI: 10.1016/j.jallcom.2015.08.240.
- [38] Boiko O., Granular metal-dielectric nanocomposites as an alternative to passive SMD, Przegląd Elektrotechniczny, vol. 1, no. 12, pp. 160–163 (2020), DOI: 10.15199/48.2020.12.32.
- [39] Radoń A., Łukowiec D., Kremzer M., Mikuła J., Włodarczyk P., *Electrical Conduction Mechanism and Dielectric Properties of Spherical Shaped Fe*₃O₄ *Nanoparticles Synthesized by Co-Precipitation Method*, Materials, vol. 11, no. 5, 735 (2018), DOI: 10.3390/ma11050735.
- [40] Rashmi, Sailaja R.R.N., Madhu B.M., Analysis of Epoxy Nanocomposites Characteristics by Impedance Spectroscopy, Macromolecular Symposia, vol. 398, no. 1, 1900168 (2021), DOI: 10.1002/masy.201900168.
- [41] Hussain M.R., Khan Q., Khan A.A., Refaat S.S., Abu-Rub H., Dielectric Performance of Magneto-Nanofluids for Advancing Oil-Immersed Power Transformer, IEEE Access, vol. 8, pp. 163316–163328 (2020), DOI: 10.1109/ACCESS.2020.3021003.
- [42] Koutras K.N., Naxakis I.A., Antonelou A.E., Charalampakos V.P., Pyrgioti E.C., Yannopoulos S.N., Dielectric strength and stability of natural ester oil based TiO₂ nanofluids, Journal of Molecular Liquids, vol. 316, 113901 (2020), DOI: 10.1016/j.molliq.2020.113901.
- [43] Zawrah M.F., Khattab R.M., Girgis L.G., El Daidamony H., Abdel Aziz R.E., *Stability and electrical conductivity of water-base Al*₂*O*₃ *nanofluids for different applications*, HBRC Journal, vol. 12, no. 3, pp. 227–234 (2016), DOI: 10.1016/j.hbrcj.2014.12.001.
- [44] Shojaei S., Rostami-Tapeh-Esmaeil E., Mighri F., *A review on key factors influencing the electrical conductivity of proton exchange membrane fuel cell composite bipolar plates*, Polymers for Advanced Technologies, vol. 35, no. 2, e6301 (2024), DOI: 10.1002/pat.6301.
- [45] Saboktakin M.R., Maharramov A., Ramazanov M.A., Synthesis and Characterization of Superparamagnetic Polyaniline Nanocomposites as Conductive Shields, Journal of Elastomers & Plastics, vol. 43, no. 2, pp. 155–166 (2011), DOI: 10.1177/0095244310393929.
- [46] Wang T., Zhao W.X., Miao Y.K., Cui A.G., Gao C.H., Wang C., Yuan L.Y., Tian Z.N., Meng A.L., Li Z.J., Zhang M., Enhancing Defect-Induced Dipole Polarization Strategy of SiC@MoO₃ Nanocomposite Towards Electromagnetic Wave Absorption, Nano-Micro Letters, vol. 16, no. 1, 273 (2024), DOI: 10.1007/s40820-024-01478-2.
- [47] Sahu G., Das M., Yadav M., Sahoo B.P., Tripathy J., Dielectric Relaxation Behavior of Silver Nanoparticles and Graphene Oxide Embedded Poly(vinyl alcohol) Nanocomposite Film: An Effect of Ionic Liquid and Temperature, Polymers, vol. 12, no. 2, 374 (2020), DOI: 10.3390/polym12020374.